# Interannual Variations and Trends in Remotely Sensed and Modeled Soil Moisture in China

BINGHAO JIA

*State Key Laboratory of Numerical Modeling for Atmospheric Sciences and Geophysical Fluid Dynamics (LASG), Institute of Atmospheric Physics, Chinese Academy of Sciences, Beijing, China*

JIANGUO LIU

*School of Mathematics and Computational Science, and Key Laboratory of Intelligent Control Technology for Wuling-Mountain Ecological Agriculture in Hunan Province, Huaihua University, Huaihua, Hunan, China*

ZHENGHUI XIE

*State Key Laboratory of Numerical Modeling for Atmospheric Sciences and Geophysical Fluid Dynamics (LASG), Institute of Atmospheric Physics, Chinese Academy of Sciences, Beijing, China*

CHUNXIANG SHI

*National Meteorological Information Center, China Meteorological Administration, Beijing, China*

(Manuscript received 5 January 2018, in final form 10 April 2018)

ABSTRACT

In this study, a microwave-based multisatellite merged product released from the European Space Agency's Climate Change Initiative (ESA CCI) and two model-based simulations from the Community Land Model 4.5 (CLM4.5) and Global Land Data Assimilation System (GLDAS) were used to investigate interannual variations and trends of soil moisture in China between 1979 and 2010. They were also evaluated using in situ observations from the nationwide agrometeorological network. These three datasets show consistent drying trends for surface soil moisture in northeastern and central China, as well the eastern portion of Inner Mongolia, and wetting trends in the Tibetan Plateau, which are also identified by in situ observations. Trends in the root-zone soil moisture are in line with those of surface soil moisture seen in the CLM4.5 and GLDAS simulations obtained from most areas in China (78%–88%), except for northwestern China and southwest of the Tibetan Plateau. Moreover, the drying trend intensifies with increasing soil depth. Taking the in situ measurements as reference, it is found that ESA CCI has better accuracy in identifying the significant drying trends while CLM4.5 and GLDAS capture wetting trends better. Compared to temperature, precipitation is the primary factor responsible for these trends, which controls the direction of soil moisture changes, while increasing temperatures can also enhance soil drying during periods of decreased precipitation.

## 1. Introduction

Soil moisture is a key variable for numerical weather prediction and climate forecasting because it controls the partitioning of energy into latent and sensible heat fluxes at the soil–atmosphere surface (Wang et al. 2011; Y. Liu et al. 2016). Many applications require large-scale soil moisture information, to be used as realistic initial states for the soil moisture variables, from weather forecasts and seasonal climate predictions to models of plant growth and carbon fluxes and drought monitoring (Albergel

Denotes content that is immediately available upon publication as open access.

Supplemental information related to this paper is available at the Journals Online website: https://doi.org/10.1175/JHM-D-18-0003.s1.

*Corresponding author*: J. Liu, jgliu@mail.iap.ac.cn

DOI: 10.1175/JHM-D-18-0003.1

et al. 2012; Dai 2013; Zhan et al. 2016). Because of the high spatial variability of soil moisture and sparse in situ measurement sites, it is not possible to generate accurate soil moisture estimates at global or continental scales from ground-based observations.

One way to estimate surface soil water content at large scales is to rely on microwave remote sensing satellites, which can provide quantitative information about the water content of a shallow surface layer as well as offering global coverage and good temporal resolution (Njoku et al. 2003; Albergel et al. 2013a). Moreover, microwave-based observations are available under cloudy weather and at nighttime. A number of microwave-based soil moisture products have been produced using passive or active microwave sensors, for example, the Advanced Microwave Scanning Radiometer for Earth Observing System (AMSR-E; Njoku et al. 2003) and Advanced Scatterometer (ASCAT; Bartalis et al. 2007). However, none of the individual microwave products covers the minimum time period of 30 years in order to be considered as a climate data record (Dorigo et al. 2015). A first attempt to utilize the synergy between different active and passive microwave products and merge them into a multidecadal satellite-based global soil moisture dataset [the European Space Agency's Climate Change Initiative (ESA CCI)] was made by Liu et al. (2011, 2012). Much of the research over the past 5 years has examined the performance of the ESA CCI over different areas (Albergel et al. 2013b; Dorigo et al. 2015, 2017; Lai et al. 2016; Jia et al. 2015), which enables the application of satellite soil moisture in drought monitoring (Yuan et al. 2015) and surface trend analyses (Dorigo et al. 2012; Albergel et al. 2013b; Loew et al. 2013; Feng and Zhang 2015; Chen et al. 2016; Rahmani et al. 2016; Su et al. 2016).

Another way to produce accurate surface and root-zone soil moisture estimates at regional or global scales is to rely on land surface models (LSM). Numerical simulations have been used as an effective tool to investigate the spatial–temporal evolution (Lai et al. 2016; Jia et al. 2015) and long-term trends of soil moisture (Li et al. 2011; Wang et al. 2011). However, the accuracy of model-based soil moisture is dependent on the quality of the meteorological forcing data (Wang and Zeng 2011; Liu and Xie 2013) and the physical parameterizations (Wang et al. 2011; Huang et al. 2013). A third way is to combine both remotely sensed surface soil moisture and model estimates through data assimilation (Albergel et al. 2012; de Rosnay et al. 2013).

China, as the world's third-largest country in land area and one of the world's most populous regions, is sensitive to climate change and has diverse climates and vegetation types, which leads to large spatial and temporal variations in soil moisture (Huang et al. 2014). Modeling results from the Community Land Model version 3.5 (CLM3.5), forced by an observation-based meteorological field, revealed a wetting trend in arid and humid regions and a drying trend in semiarid regions of China (Li et al. 2011). Next, the long-term dataset from the Global Land Data Assimilation System (GLDAS) exhibited a clear decreasing trend in most parts of northern China (Cheng et al. 2015). Several studies have used the ESA CCI product to assess soil moisture trends in China (Li et al. 2015; An et al. 2016; Chen et al. 2016; Zheng et al. 2016), even in comparison with in situ observations (Wang et al. 2016) and LSMs (Qiu et al. 2016). They found that the ESA CCI product shows consistent soil moisture trends with in situ observations, with drying in northwestern China (Li et al. 2015), the north China plain (Qiu et al. 2016), and northeast China (Wang et al. 2016). Qiu et al. (2016) even pointed out that the ESA CCI product captures surface soil moisture trends of in situ measurements more accurately than the land surface reanalysis dataset ERA-Interim/Land. However, few studies examined the differences of soil moisture trends in China derived from LSMs and satellite products (Qiu et al. 2016), since most previous research focused on the global scale (Dorigo et al. 2012; Albergel et al. 2013b; Loew et al. 2013) or other regions, for example, Iran (Rahmani et al. 2016). In addition, there appears to be a lack of investigations on the discrepancy between surface and root-zone soil moisture trends in China. Moreover, discussions regarding the response of soil moisture trends of China derived from different soil depths to climate change are not well presented.

In this paper, we investigate interannual variations and trends of soil moisture in mainland China based on three soil moisture datasets: the ESA CCI data product and model simulations from CLM4.5 and GLDAS. The results are evaluated using in situ observations from 306 sites. Moreover, the response of the soil moisture temporal variability to climate change is discussed, which is important for deepening our understanding of the interaction of soil moisture with the Earth system.

## 2. Data and methodology

### a. *CLM4.5*

CLM is a community-developed LSM by a grassroots collaboration of scientists who have an interest in making a general land surface model available for public use (Dai et al. 2003). CLM4.5, released by the National Center for Atmospheric Research, is the latest version and contains several new modifications relative to previous releases, including updates to canopy and hydrology processes (Oleson et al. 2013). In CLM4.5, soil moisture calculations are performed over 15 layers with different soil depths representing a total column of

around 42 m. In this study, we ran CLM4.5 over China (15°–55°N, 70°–140°E) with an observation-based forcing dataset developed by the Institute of Tibetan Plateau Research, Chinese Academy of Sciences (hereafter ITP). This dataset was constructed by combining ground measurements from 740 operational field sites of the China Meteorology Administration (CMA), a satellite-based precipitation product (Chen et al. 2011), the incident shortwave radiation data produced by Yang et al. (2010), and meteorological data from GLDAS (Rodell et al. 2004). The spatial and temporal resolutions of the ITP data are 0.1° × 0.1° and 3-hourly, respectively. For the CLM4.5 simulations, we first spun up the model for 300 years by repeating 30-yr (1979–2008) ITP data to achieve an equilibrium state, and then we used the atmospheric forcing data of 1979–2012 to run CLM4.5 to obtain the simulated results. CLM4.5 was run with a spatial resolution of 0.25° × 0.25° and a half-hourly temporal resolution. Note that the ITP data were bilinearly interpolated to the 0.25° grid and surface parameters used in this study are the default values recommended by the CLM4.5 (Oleson et al. 2013).

### b. GLDAS data

The GLDAS product was developed jointly by the National Aeronautics and Space Administration's Goddard Space Flight Center and the National Oceanic and Atmospheric Administration's National Centers for Environmental Prediction. It was designed to ingest satellite and ground-based observational data products using advanced land surface modeling and data assimilation techniques (Rodell et al. 2004). GLDAS version 2.0 was used in this study by ingesting monthly data from the Noah model (Chen et al. 1996), which was forced with the Princeton meteorological dataset (Sheffield et al. 2006). It had a spatial resolution of 0.25° between 1979 and 2010. The Noah model has four soil layers with ranges of 0–10, 10–40, 40–100, and 100–200 cm, and the unit of soil moisture has been changed to volumetric content ($m^3 m^{-3}$).

### c. ESA CCI soil moisture data

The ESA CCI soil moisture product is a merged multisatellite microwave soil moisture dataset, which is a combination of passive products from the Scanning Multichannel Microwave Radiometer (SMMR), the Special Sensor Microwave Imager (SSM/I), the Tropical Rainfall Measuring Mission Microwave Imager (TMI), AMSR-E, the WindSat radiometer (WindSat), and the Advanced Microwave Scanning Radiometer-2 (AMSR2), and active products from Scatterometer (SCAT) and ASCAT (Liu et al. 2011, 2012). ESA CCI version 2.1, released by the Vienna University of Technology in July 2014, was used in this study. It is a blended product with global coverage and high resolution, with a spatial resolution of 0.25° × 0.25° ($m^3 m^{-3}$) and a daily time step (Liu et al. 2012).

### d. Ground-based soil moisture, precipitation, and temperature measurements

Ground-based measurements of soil moisture from agricultural meteorological stations of the CMA across China were chosen in this study to evaluate soil moisture trends. These observations were obtained three times each month (i.e., on days 8, 18, and 28) using the gravimetric technique and were available during the growing season (March–October). The postprocessed monthly volumetric soil water content data at 306 stations between 1993 and 2010, which were obtained using the quality-control method proposed by Jia et al. (2015), were employed here. It is noted that if more than one in situ station occurred in a single 0.25° grid box, a correlation check method was adopted to remove any redundant sites (Dorigo et al. 2015). Our method is as follows: we first calculated the correlation coefficients between the in situ measurements and three soil moisture (SM) datasets (ESA CCI, CLM4.5, GLDAS), respectively, and their average value was compared for each site, after which the site with the highest average correlation was retained.

To compare with the precipitation and temperature changes from the ITP and GLDAS datasets, the ground-based monthly gridded (0.5° × 0.5°) precipitation and temperature data provided by the National Meteorological Information Center (NMIC) of CMA were chosen as observations. To be consistent with other datasets used in this study, they were bilinearly interpolated to a 0.25° grid. This dataset was generated based on 2472 meteorological stations using the thin plate smooth spline method (Zhao et al. 2014), where the Global 30-arc-s elevation (GTOPO30) DEM data were used to eliminate the influence of complex elevation (http://data.cma.cn).

### e. Analysis strategy

Before the trend analysis, daily values of all three datasets (CLM4.5, GLDAS, and ESA CCI) were converted to monthly time series and then averaged for the growing season (March–October) to construct the annual mean. The same processing was applied to precipitation and temperature data. The nonparametric Mann–Kendall method was performed to determine the statistical significance of trends, where the Sen median slope was considered as the trend values in this paper.

We first test for statistical significance of trends by computing the Mann–Kendall statistic $S$. Each data value is compared with all subsequent data values:

$$S = \sum_{k=1}^{n-1} \sum_{j=k+1}^{n} \mathrm{sgn}(\mathrm{SM}_j - \mathrm{SM}_k) \quad \text{and} \quad (1)$$

$$\mathrm{sgn}(\mathrm{SM}_j - \mathrm{SM}_k) = \begin{cases} 1, & \mathrm{SM}_j > \mathrm{SM}_k \\ 0, & \mathrm{SM}_j = \mathrm{SM}_k \\ -1, & \mathrm{SM}_j < \mathrm{SM}_k \end{cases}, \quad (2)$$

where $n$ is the length of the record at a given grid cell or in situ site. The variance of $S$ [Eq. (3)] is then calculated to test for the presence of a statistically significant trend using the $Z$ value [Eq. (4)]:

$$\mathrm{var}(S) = \frac{1}{18}\left[n(n-1)(2n+5) - \sum_{p=1}^{q} t_p(t_p-1)(2t_p+5)\right]$$

and (3)

$$Z = \begin{cases} \dfrac{S-1}{\sqrt{\mathrm{var}(S)}}, & S > 0 \\ 0, & S = 0 \\ \dfrac{S+1}{\sqrt{\mathrm{var}(S)}}, & S < 0 \end{cases}. \quad (4)$$

Here $q$ is the number of tied groups, and $t_p$ is the number of data values in the $p$th group. The statistic $Z$ is compared with a tolerable probability (the default significance level is set as 0.05 in this study). If a linear trend is statistically significant, then the change per unit of time is estimated by using a simple nonparametric procedure developed by Sen (1968):

$$b_{\mathrm{sen}} = \mathrm{median}\left(\frac{\mathrm{SM}_j - \mathrm{SM}_k}{j-k}\right), \qquad j > k. \quad (5)$$

If there are $n$ values of $\mathrm{SM}_j$ in the time series, we get as many as $n(n-1)/2$ slope estimates, and $b_{\mathrm{sen}}$ is taken as their median.

The multiple linear regression method was used to quantify the contributions of the climate factors (e.g., precipitation, temperature, solar radiation) $X_i$ ($i = 1, 2, \ldots, n$), to the trend in soil moisture $S$. First, we obtained the regressed soil moisture based on the annual mean climate data at each grid point:

$$S = \sum_{i=1}^{n} a_i \times X_i + \varepsilon, \quad (6)$$

where $a_i$ ($i = 1, 2, \ldots, n$) is the regression coefficient, and $\varepsilon$ is the residual error term. Then, the contributions of the change in climate factors $C_i$ ($i = 1, 2, \ldots, n$) to the change in soil moisture were obtained as follows:

$$C_i = (a_i \times \Delta X_i)/\Delta S \times 100\%, \quad (7)$$

where $\Delta S$ and $\Delta X_i$ are the respective changes in the mean values of $S$ and $X_i$ between the first and last values in a 5-yr interval. It is noted that the estimated contributions from climate factors are based on a multiple linear regression by assuming that these climate variables are independent from each other, while in reality they are sometimes correlated.

## 3. Results

### a. *Spatial distribution and interannual variation of soil moisture in China*

First, we used the model simulations and satellite products to examine the spatial patterns of soil moisture. Figure 1 shows the spatial distributions of the mean ESA CCI and surface soil moisture (0–10 cm) from CLM4.5 and GLDAS averaged between 1979 and 2010, together with the associated climate variables that affect soil moisture, including observed precipitation and temperature (section 2d). Note that the 0–10-cm soil moisture of CLM4.5 is a weighted average value based on the top four soil layer thicknesses (1.75, 2.76, 4.55, and 7.50 cm, respectively). Their weights are 0.175, 0.276, 0.455, and 0.094, respectively. It can be seen from Fig. 1 that all three soil moisture datasets show similar broad patterns, with obvious northwest–northeast and northwest–southeast gradients from dry to wet. This is consistent with the spatial patterns of precipitation, which has an obvious northwest–southeast increasing gradient, except for northeastern China, in which wet soil has a close relation with low temperature and dense vegetation. In addition, the three soil moisture products have high spatial correlation coefficients ranging between 0.95 and 0.98 (Table 1) among which ESA CCI and GLDAS have the highest spatial similarity since the ESA CCI product was recalled against GLDAS using the cumulative distribution function (CDF) matching technique (Liu et al. 2012). Compared to GLDAS, CLM4.5 shows wetter soil in northeastern China and drier soil in the Tibetan Plateau and southern parts of China. ESA CCI has lower soil moisture than the two simulated model results.

As shown in Fig. 2a, the annual mean temperature in China shows a consistently rapid warming trend (0.032°–0.040°C yr$^{-1}$, significant at the 95% level) for the three datasets, and a hiatus can be seen since 2000. Different from the temperature, the three precipitation datasets

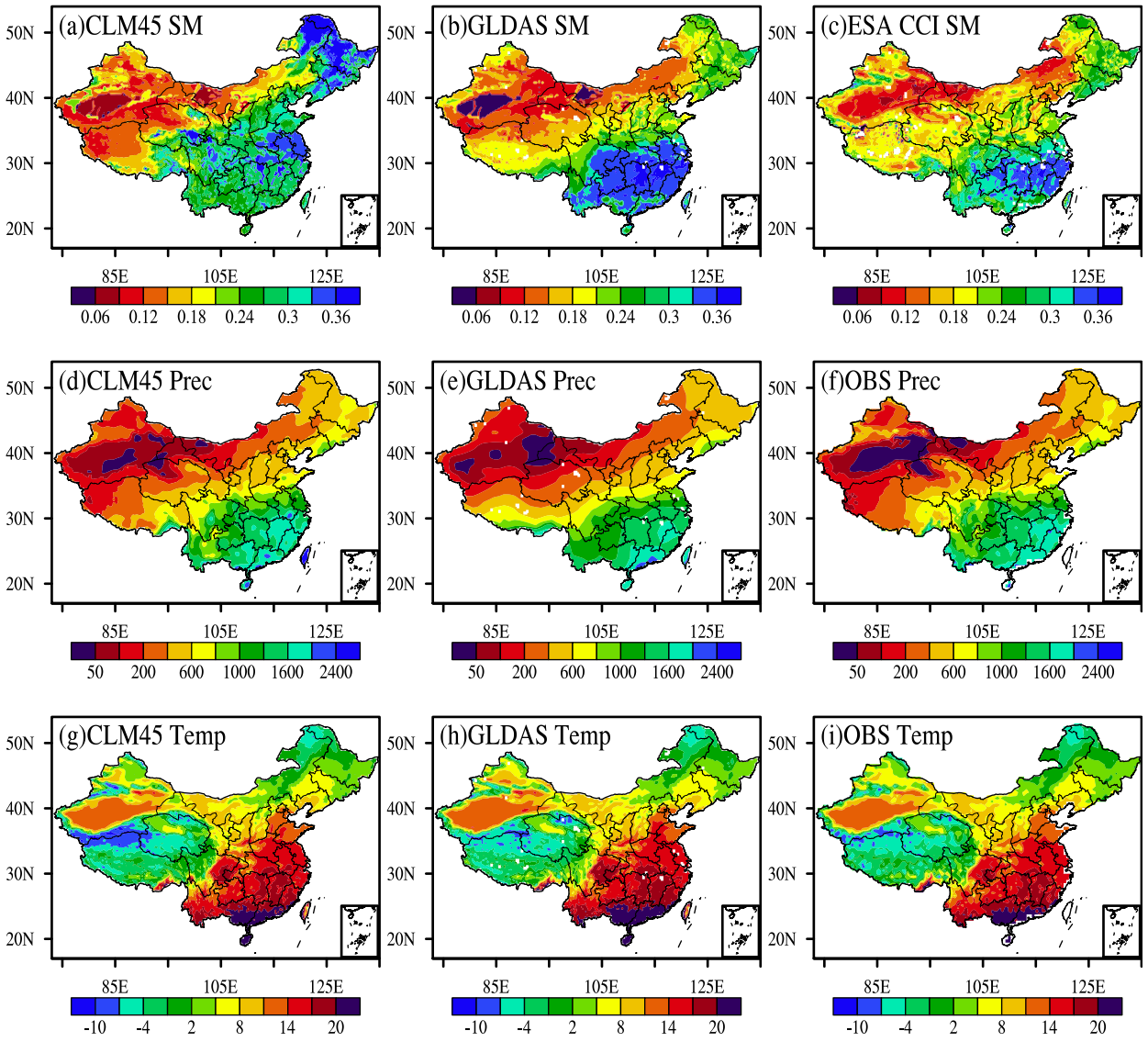


FIG. 1. Spatial distributions of annual mean (a)–(c) soil moisture ($m^3\,m^{-3}$), (d)–(f) precipitation (Prec; mm), and (g)–(i) temperature (Temp; °C) between 1979 and 2010. OBS represents the ground-based gridded precipitation and temperature observations.

show large differences (Fig. 2b). The ITP precipitation increases significantly (2.49 mm $yr^{-1}$), while both the ground-based observations (OBS) and the GLDAS data change very little; however, they all show a clear decrease between 2003 and 2004 and an abrupt increase in 2008. Interannual variations of the surface and root-zone soil moisture anomaly in China are presented in Figs. 2c and 2d, respectively.

The three datasets show a consistent decreasing trend in surface soil moisture during the past 32 years (1979–2010), although only the trend of GLDAS is statistically significant ($p < 0.05$) due to increased air temperature and decreased precipitation (blue line). CLM4.5 shows a slightly higher drying trend in deep soil (200 cm) than that of surface soil (10 cm). In contrast, there is a clearly enhanced soil drying trend with an increase in soil layer thickness seen in the GLDAS simulation (Fig. 2d). Since soil moisture derived from both the model simulations and satellite product over many areas of China did not show significant trends (see section 3b and Fig. 3), we also compared the interannual variations and trends of soil moisture averaged over only those areas with significant trends (see Fig. S1 in the online supplemental material). It is found that surface soil moisture from both the GLDAS and ESA CCI exhibit significant drying trends (Fig. S1a). Similar to that in Fig. 2d, deeper soil layers in GLDAS (Fig. S1b) appear to show enhanced drying trends compared to those at the surface.

TABLE 1. Spatial correlation coefficients of the multiyear (1979–2010) averaged soil moisture, precipitation, and temperature among CLM4.5, GLDAS, and ESA CCI.

| | | CLM4.5 | GLDAS | ESA CCI |
|---|---|---|---|---|
| Soil moisture | CLM4.5 | 1.0 | — | — |
| | GLDAS | 0.96 | 1.0 | — |
| | ESA CCI | 0.95 | 0.98 | 1.0 |
| Precipitation | CLM4.5 | 1.0 | — | — |
| | GLDAS | 0.98 | 1.0 | — |
| | ESA CCI | 0.99 | 0.98 | 1.0 |
| Temperature | CLM4.5 | 1.0 | — | — |
| | GLDAS | 0.99 | 1.0 | — |
| | ESA CCI | 0.98 | 0.98 | 1.0 |

However, for this area CLM4.5 shows a wetting trend at the surface (Fig. S1a), which is different from that averaged across China (Fig. 2c). In contrast, a weak wetting trend is detected for CLM4.5 root-zone soil moisture (0–50 cm). This switches to a (not significant, Fig. S2b) drying trend at depths up to 200 cm, suggesting that the percent area of significant drying soil from CLM4.5 increases with increasing soil depth.

### b. *Trend analysis*

Since the variability of soil moisture is spatially heterogeneous, further investigation of the spatial consistency of the long-term trend is necessary. Comparisons of the surface soil moisture trends (1979–2010) derived from CLM4.5, GLDAS, and ESA CCI are presented in Fig. 3. The significant trends are masked using shaded areas ($p < 0.05$). In general, they agree in many areas, for example, there are significant drying trends in northeastern and central China, and eastern parts of Inner Mongolia, and wetting trends in the Tibetan Plateau. CLM4.5 is dominated by increasing soil moisture content over time, where 77% of all significant trends (Fig. 3a) are wetting trends (positive values). This is mainly due to the increasing precipitation trend from the ITP forcing data over most of China, which mainly exists in northwestern China and the Tibetan Plateau (Fig. 3d). In contrast, GLDAS and ESA CCI behave differently, where 56% and 63% of all significant trends are drying, respectively. Moreover, the wetting trend seen in the eastern area of the Yellow River basin could be identified by both CLM4.5 and GLDAS, while the trend is not obvious, or is even decreasing, in the ESA CCI product.

Figure 4 presents the change in root-zone soil moisture during 1979–2010 obtained from CLM4.5 and GLDAS. Significant trends ($p < 0.05$) are represented using shaded areas: 34% (30%) of CLM4.5 and 38% (46%) of GLDAS soil moisture trends are significant for 0–50 cm (0–200 cm), which are slightly larger than those from the surface. Among them, 35% (53%) for CLM4.5 and 68% (71%) for GLDAS are drying at the 0–50 cm (0–200 cm) soil depths. It suggests that the percent area of significant drying increases with an increases in soil depth, which is consistent with the result from Fig. S2. The prominent drying trends for CLM4.5 and GLDAS mainly occur in Inner Mongolia and northeastern and central China. In addition, 88% (80%) and 83% (78%) at 0–50 cm (0–200 cm) have the same soil moisture trend tendency with that of surface soil moisture for CLM4.5 and GLDAS, respectively. The main differences between the root-zone and surface soil moisture trends are in northwest China and southwest of the Tibetan Plateau. Compared to CLM4.5, 60% and 58% of GLDAS have the same soil moisture trend for 0–50 cm and 0–200 cm, respectively, which is slightly smaller than that of 0–10 cm (63%, Fig. 3).

### c. *Comparing trends with ground-based observations*

Ground-based soil moisture observations are only available during the growing season (March–October) after 1993. A comparison of the simulated soil moisture trends with the satellite products against in situ observations between 1993 and 2010 is depicted in Fig. 5. It is noted that only the daily data of the model simulations and satellite products on the days of each month when ground measurements were available (three times each month; section 2d) and hence used to compute their monthly and yearly mean values. In addition, we used the "nearest neighbor" approach to match the grid box from the satellite-based products and model simulations with ground-based observations. It is seen from Fig. 5 that the satellite product and model simulations all show consistent and significant soil drying trends with in situ measurements between 1993 and 2010 in Inner Mongolia and northeast China, and a significant wetting trend in the western Tibetan Plateau. Additionally, a wetting soil moisture trend in parts of northwest China is also identified by the four soil moisture datasets. Table 2 shows the numbers of stations for in situ observations identified with the same level trends of those from the CLM4.5, GLDAS, and ESA CCI products, and their corresponding ratios against all in situ stations, which were detected at the same level trends. It is found that CLM4.5 and GLDAS agree better with ground observations than ESA CCI for all available in situ stations with wetting trends (significant and nonsignificant). However, ESA CCI captures the significantly drying trends of in situ observations better (37.5%) than CLM4.5 (4.2%) and GLDAS (20.8%). These in situ stations are mainly located in arid and semiarid regions. In addition, ground-based measurements show a noticeable increasing trend in the western areas of the Yellow River basin, which are also detected by ESA CCI. The two land surface models show

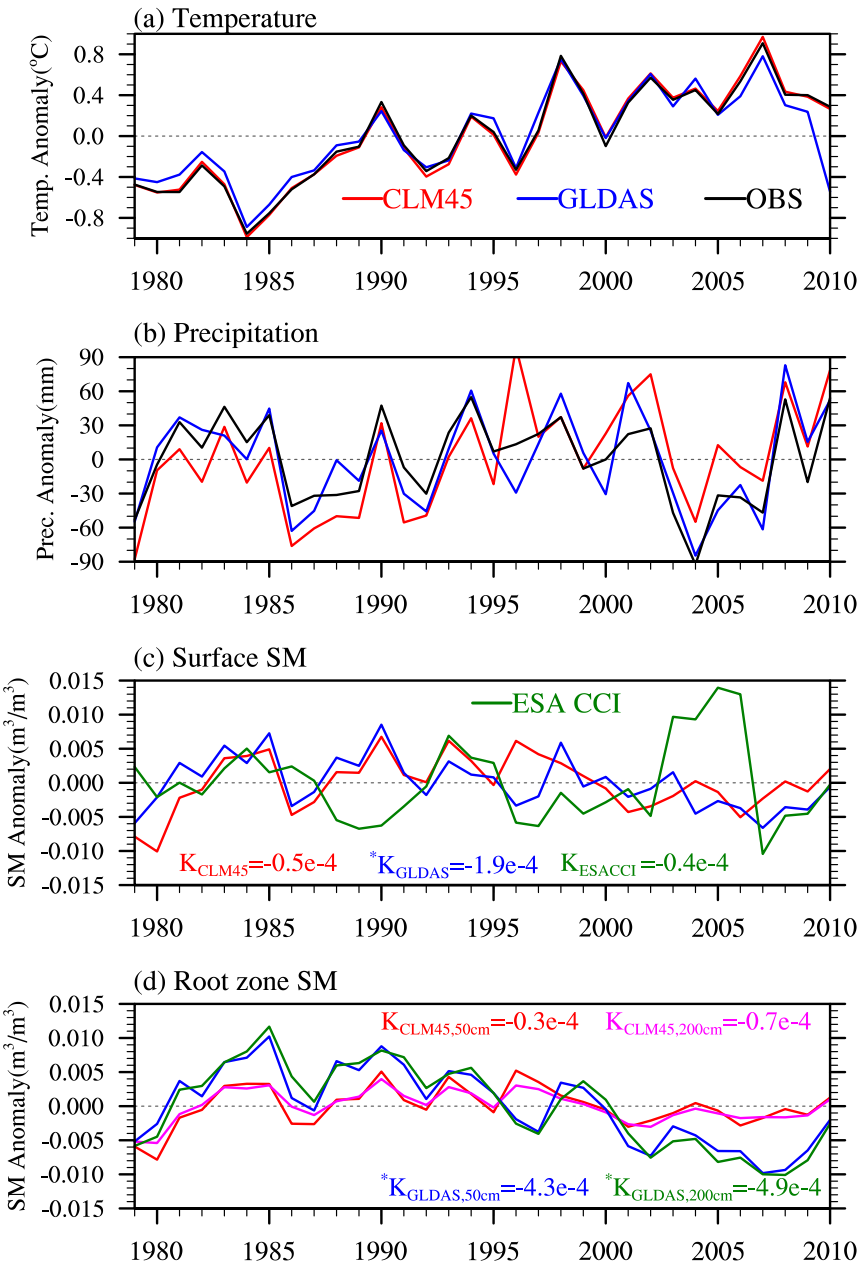


FIG. 2. Annual mean (a) temperature, (b) precipitation and (c) surface (0–10 cm) and (d) root-zone SM anomalies (0–50 and 0–200 cm) averaged over China between 1979 and 2010. Parameter $K$ is the soil moisture trend ($m^3\,m^{-3}\,yr^{-1}$) calculated using the Mann–Kendall test method. The asterisk represents the statistically significant trends ($p < 0.05$).

large differences with ground-based observations in this region. These suggest that ESA CCI has a high quality over arid–semiarid areas (Dorigo et al. 2015, 2017; Jia et al. 2015).

The Huang-Huai-Hai (HHH) Plain (Fig. 5b) is regarded as the ''Granary of China'' and is one of the most intensively irrigated regions in the world (Shi et al. 2014; Qiu et al. 2016). It mainly covers the eastern area of the Yellow River basin (III), and most parts of the Haihe River (II) and Huaihe River basins (IV). Ground-based observations show a clearly increasing trend in the HHH Plain (Fig. 5a), whereas 65% of all in situ sites are identified as having a wetting trend (29% is significant and 36% is nonsignificant). Especially in the Haihe River basin, 35% of in situ sites were detected with significantly increasing trends. Since precipitation did

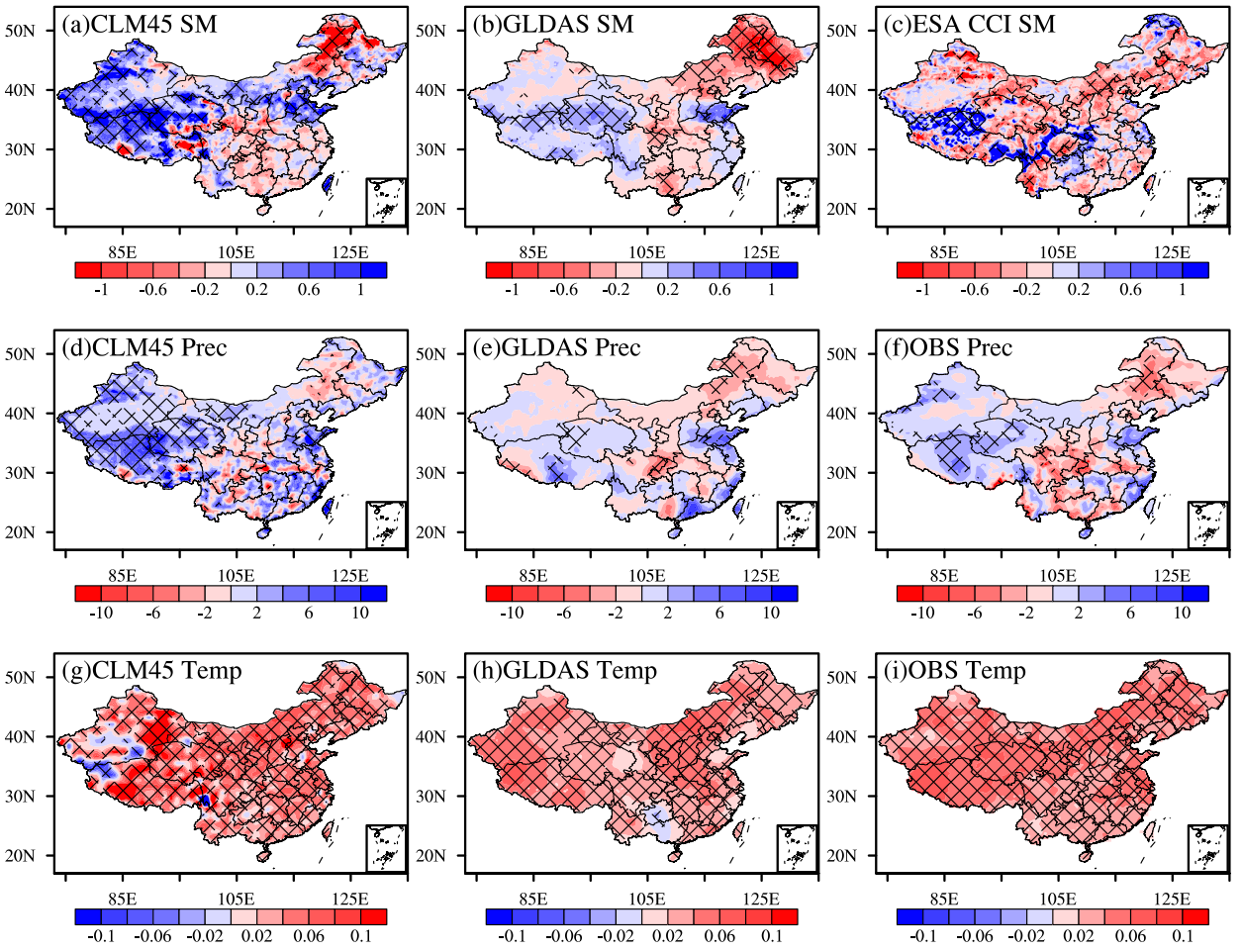


FIG. 3. The spatial distributions of linear trends for annual mean (a)–(c) surface SM ($10^{-3}$ m$^3$ m$^{-3}$ yr$^{-1}$), (d)–(f) precipitation (mm yr$^{-1}$), and (g)–(i) temperature (°C yr$^{-1}$) between 1979 and 2010. OBS represents the ground-based gridded precipitation and temperature observations. The shaded areas show grids with statistically significant trends ($p < 0.05$).

not change significantly in this area during the study period, the significant wetting trend may be related to massive anthropogenic interference with the local water resources, including excessive groundwater extraction (Qiu et al. 2016) and interbasin water transfer (Chen and Xie 2010). CLM4.5 shows increasing trends in most parts of the HHH Plain (Fig. 5b), while only the Huaihe River basin shows a wetting trend for GLDAS (Fig. 5c). On the contrary, ESA CCI shows drying trends in most of the in situ locations except for the southeast of the Haihe River basin and the middle of the Huaihe River basin. The statistical results of the agreement between the three datasets and in situ observations in the HHH Plain are presented in Table 2 (right column). It can be seen that, if taking the in situ observations as benchmark, CLM4.5 has better accuracy in identifying the wetting trend in the HHH Plain while GLDAS (52.6%) and ESA CCI (63.2%) capture the drying trend better. In the Yunnan province of southwestern China, many areas are covered by rain forest and evergreen trees, and CLM4.5 and GLDAS detected consistent decreasing trends with ground-based observations; however, ESA CCI shows contrasting trends. This indicates that the satellite product cannot effectively capture temporal variations of soil moisture in densely vegetated areas.

### *d. Interannual variations and trends in major river basins*

To investigate the regional-scale interannual variability and trends in soil moisture, Fig. 6 illustrates the temporal evolution of the annual soil moisture anomalies in the eight major river basins of China (Fig. 5a) from 1979 to 2010. The results show that the three datasets display consistent interannual variations in most of the basins, except that ESA CCI shows large changes in 1988 (Figs. 6a,h) and in 2006 (Figs. 6a,g,h) in the Songhuajiang, Yangze, and Zhujiang River basins. This is may be related to the resampling and scaling strategy

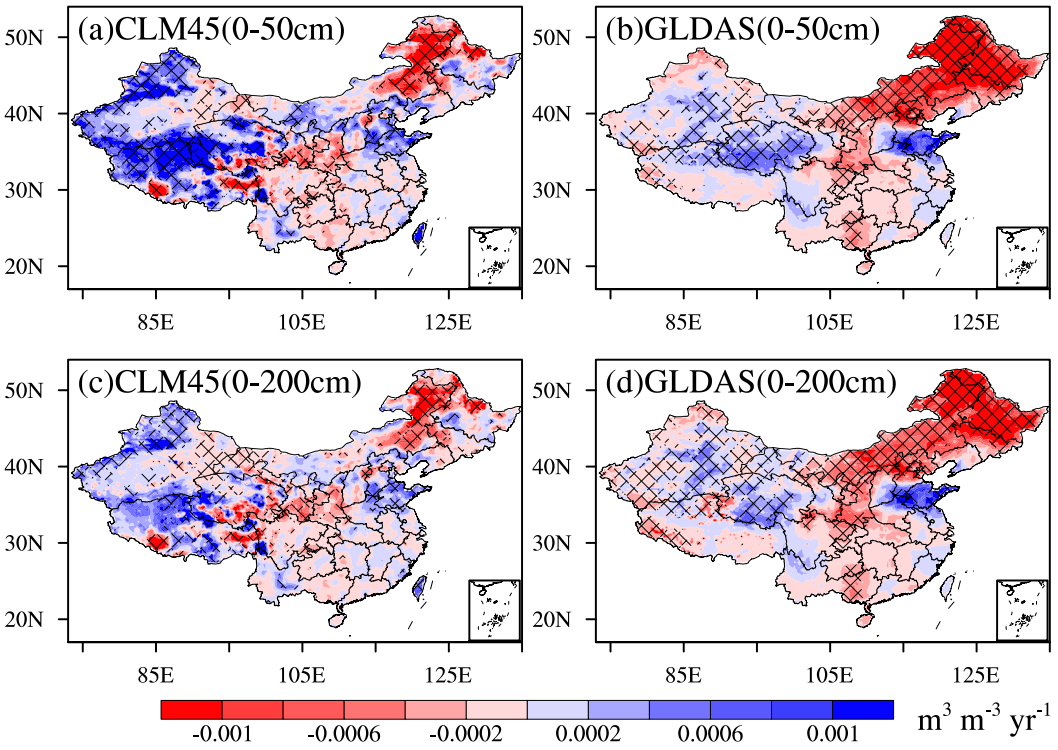


FIG. 4. The spatial distribution of linear trends for annual mean soil moisture ($m^3\,m^{-3}\,yr^{-1}$) derived from (left) CLM4.5 and (right) GLDAS between 1979 and 2010 in the root zone for (a),(b) 0–50 and (c),(d) 0–200 cm. The shaded areas show grids with statistically significant trends ($p < 0.05$).

used to incorporate the SSM/I and ASCAT products. In addition, they exhibit some differences in the soil moisture trends throughout the period, except for the Songhuajiang River basin. GLDAS detects drying trends in surface soil moisture in all the basins except the Tarim (Fig. 6f) and Yellow River basins (Fig. 6c), while CLM4.5 shows wetting trends in most of the eight basins except for the Songhuajiang and Zhujiang River basins. In contrast, ESA CCI shows the same trends with GLDAS except for the Songhuajiang River basin. In addition, the interannual variations and trends of soil moisture averaged over only those grids with significant trends were also compared at each river basin (Fig. S2). It is found that soil moisture in Fig. S2 shows the same soil moisture trend tendency with those in Fig. 2, except for a few differences in the magnitude, especially for CLM4.5. For example, CLM4.5 shows significant wetting trends in the Huai, Yangtze, and Zhujiang River basins but nonsignificant trends in Fig. 6, which were averaged over all the grids of the corresponding basin.

### e. *Contribution of climate change on soil moisture trends*

To investigate the effects of changes in precipitation and temperature on soil moisture trends, the relationship between soil moisture with precipitation and temperature is shown in Fig. 7. In general, both CLM4.5 and GLDAS have similar results, whereby drying (wetting) trends in soil moisture that are significant at the 0.05 level are mainly associated with negative (positive) precipitation trends. This indicates that precipitation trends control the direction of soil moisture change. This phenomenon was also found for other regions, such as North America, West Africa, and northern Europe (Sheffield and Wood 2008). In addition, as shown in the top-left portions of Figs. 7a and 7b, temperature warming amplifies the effect of decreasing precipitation on soil drying through an increase in evaporation, which implies that soil drying is driven primarily by a lack of precipitation, but is also accentuated by associated increases in temperature. However, the relationship between increasing temperature and soil moisture is not explicit as the controlling factor of soil evaporation and may differ for various climate regions (Seneviratne et al. 2010).

We then investigated the quantitative effects of precipitation and temperature on the soil moisture trends using the multiple regression approach [Eqs. (6)–(7)], and their relative contributions are presented in Fig. 8. In general, the contribution is dominated by precipitation in the Tibetan Plateau and northwestern China and by

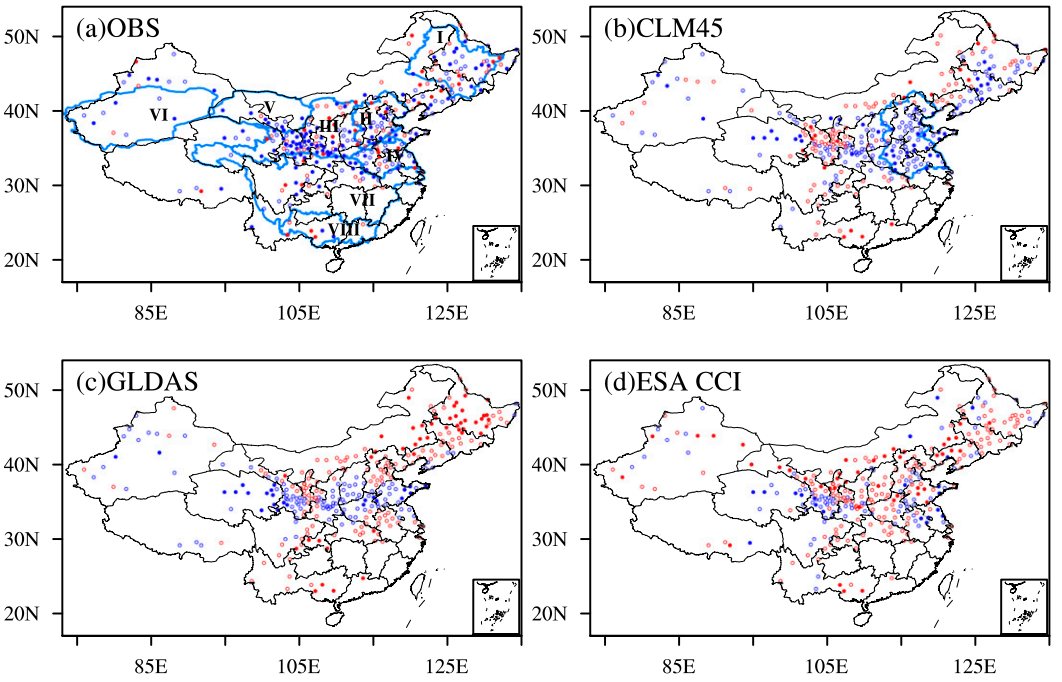


FIG. 5. Linear trends for annual mean soil moisture derived from (a) ground-based observations (OBS), (b) CLM4.5, (c) GLDAS, and (d) ESA CCI during the growing season (March–October) between 1993 and 2010 at 306 stations. The dots are statistically significant trends ($p < 0.05$), while the circles are nonsignificant; the blue represents wetting trends, while the red is for drying trends. The light blue lines in (a) are the eight major river basins in China: I, Songhuajiang River basin; II, Haihe River basin; III, Yellow River basin; IV, Huaihe River basin; V, Heihe River basin; VI, Tarim River basin; VII, Yangtze River basin; and VIII, Zhujiang River basin. The light blue line in (b) is the HHH Plain.

temperature in southern China, and the contributions of the precipitation and temperature in northeastern China are roughly equivalent. The averaged mean contribution of precipitation on significant soil moisture wetting (drying) in China for CLM4.5, GLDAS, and ESA CCI is about 82% (37%), 80% (49%), and 60% (34%), respectively, while those of the temperature are 18% (63%), 20% (51%), and 40% (66%). This means that increasing temperature has a larger influence on the soil drying trend during periods of decreased precipitation. It should be noted that the qualitative analysis and quantitative contribution show large discrepancies between the satellite products and the model simulations. One reason is that the observation-based climate data (precipitation and temperature) and satellite soil moisture products are generated from different sources, while the two simulations are consistent with their own meteorological forcing datasets. On the other hand, the two process-based models (CLM4.5 and Noah) did not consider human activities (e.g., irrigation; Zeng et al. 2016), while this effect may have been observed by the remote sensing satellites (Chen et al. 2016; Qiu et al. 2016).

Besides precipitation and temperature, other climate variables also have indirect effects on the temporal variations of soil moisture. For instance, surface solar radiation, relative humidity and wind speed are three important drivers for the land surface water cycle

TABLE 2. Numbers of stations for in situ observations identified with the same level trends of those from CLM4.5, GLDAS, and ESA CCI products in China and the HHH Plain, respectively. Their corresponding ratios against all the in situ stations, which were detected at the same level trends, are shown in the parentheses.

| | | China | HHH[a] |
|---|---|---|---|
| CLM4.5 | Wetting | 134 (65.4%) | 36 (100.0%) |
| | Drying | 47 (46.5%) | 2 (10.5%) |
| | Significantly wetting[b] | 17 (14.4%) | 6 (37.5%) |
| | Significantly drying | 1 (2.9%) | 0 |
| GLDAS | Wetting | 104 (50.7%) | 18 (50.0%) |
| | Drying | 73 (72.3%) | 10 (52.6%) |
| | Significantly wetting | 8 (6.8%) | 1 (6.25%) |
| | Significantly drying | 5 (14.7%) | 0 |
| ESA CCI | Wetting | 73 (35.6%) | 16 (44.4%) |
| | Drying | 67 (66.3%) | 12 (63.2%) |
| | Significantly wetting | 7 (5.9%) | 1 (6.3%) |
| | Significantly drying | 9 (26.5%) | 1 (20%) |

[a] HHH is the Huang-Huai-Hai Plain shown in Fig. 5b (light blue line).
[b] Significant at $p < 0.05$.

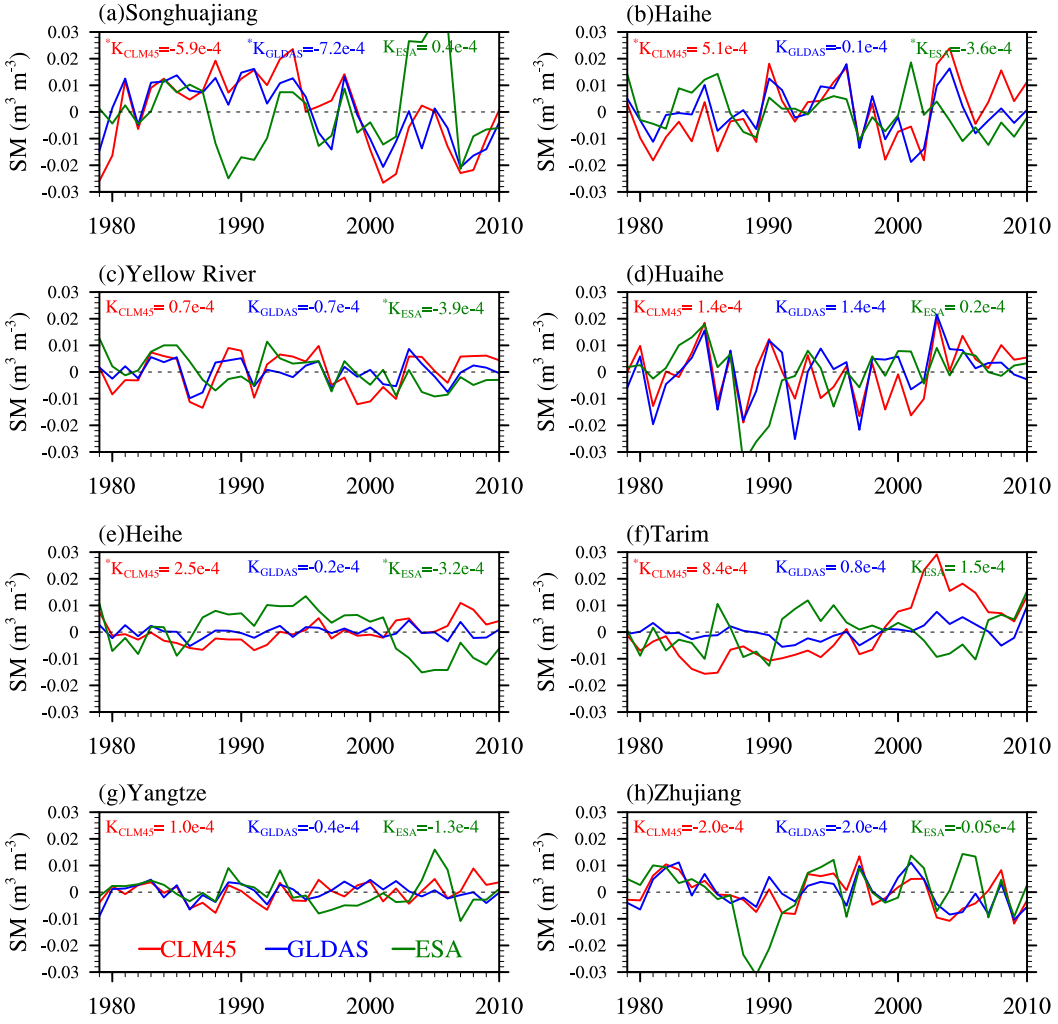


FIG. 6. Comparison of annual surface soil moisture (0–10 cm) derived from the CLM4.5 and GLDAS and the ESA CCI product over the eight major river basins of China. Parameter $K$ is the soil moisture trend ($m^3\,m^{-3}\,yr^{-1}$) calculated using the Mann–Kendall test method. The asterisk represents the statistically significant trends ($p < 0.05$).

through their link to the evapotranspiration (Guo et al. 2006; Robock and Li 2006; Seneviratne et al. 2010; J. Liu et al. 2016). The relative contributions of all the five climate variables (precipitation, temperature, solar radiation, relative humidity, and wind speed) on soil moisture trends are presented in Fig. 9 using a similar method as in Fig. 8. Different from Fig. 8, only the dominant climate factor (maximum contribution) for each grid is shown in Fig. 9. Even though five climate factors were considered in the multiregression equations [Eqs. (6)–(7)], precipitation was still found to be the dominant climate driver on the soil moisture trend over northwestern China and the western part of the Tibetan Plateau (Figs. 9a–9c) while temperature made main contributions over southern China (Figs. 9d–9f). Compared to precipitation and temperature, solar radiation provides a main contribution over parts of northern China while wind speed contributes for parts of northeast China. It further suggests that precipitation and temperature are the most important climate variables determining soil moisture trends over China.

## 4. Conclusions and discussion

In this study, the interannual variations and trends in soil moisture in China between 1979 and 2010 were investigated using a microwave-based merged satellite product (ESA CCI) and two process-based model simulations (CLM4.5 and GLDAS). Trends in soil moisture were calculated using the nonparametric Mann–Kendall trend test and evaluated against ground-based observations. We also examined the relationship of soil moisture trends with precipitation and temperature using qualitative and quantitative methods.

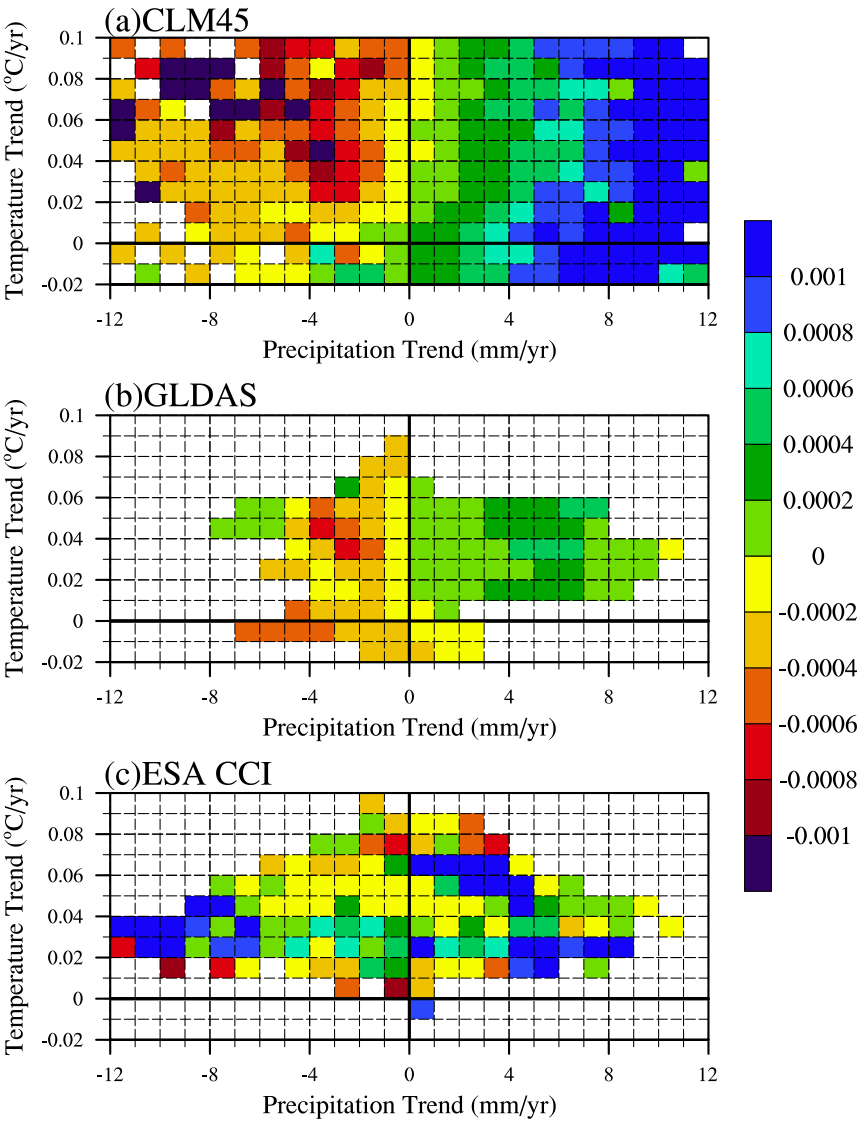


FIG. 7. Trends of soil moisture ($m^3\,m^{-3}\,yr^{-1}$) as a function of precipitation ($mm\,yr^{-1}$) and temperature trends ($°C\,yr^{-1}$). The red (blue) boxes are drying (wetting) soil moisture trends, and blank boxes indicate no data.

Both the satellite product and model simulations show significant drying trends for surface soil moisture in northeastern and central China and eastern parts of Inner Mongolia, while wetting trends were seen in the Tibetan Plateau, which were also identified by in situ observations. The root-zone soil moisture of CLM4.5 and GLDAS shows consistent trends with that of surface soil moisture in most areas of China (78%–88%), except in northwest China and southwest of the Tibetan Plateau. In addition, the percentage of areas with significant drying trends increases with an increase of soil depth.

Our analysis shows that precipitation is the primary factor responsible for the soil moisture trends reported here. During periods of decreased precipitation, temperature warming would enhance soil drying. Quantitative analysis suggests the soil moisture trends are dominated by precipitation in the Tibetan Plateau and northwest China and by temperature in southern China, and the influence of precipitation and temperature are roughly equivalent in northeastern China. In contrast, solar radiation makes a main contribution over parts of northern China while wind speed contributes for parts of northeast China.

It is noted that the analysis of the temporal evolutions of soil moisture in the present study is subject to some limitations. The in situ observations used in this study represent average soil moisture values between 0 and 10 cm using the gravimetric technique. To be consistent

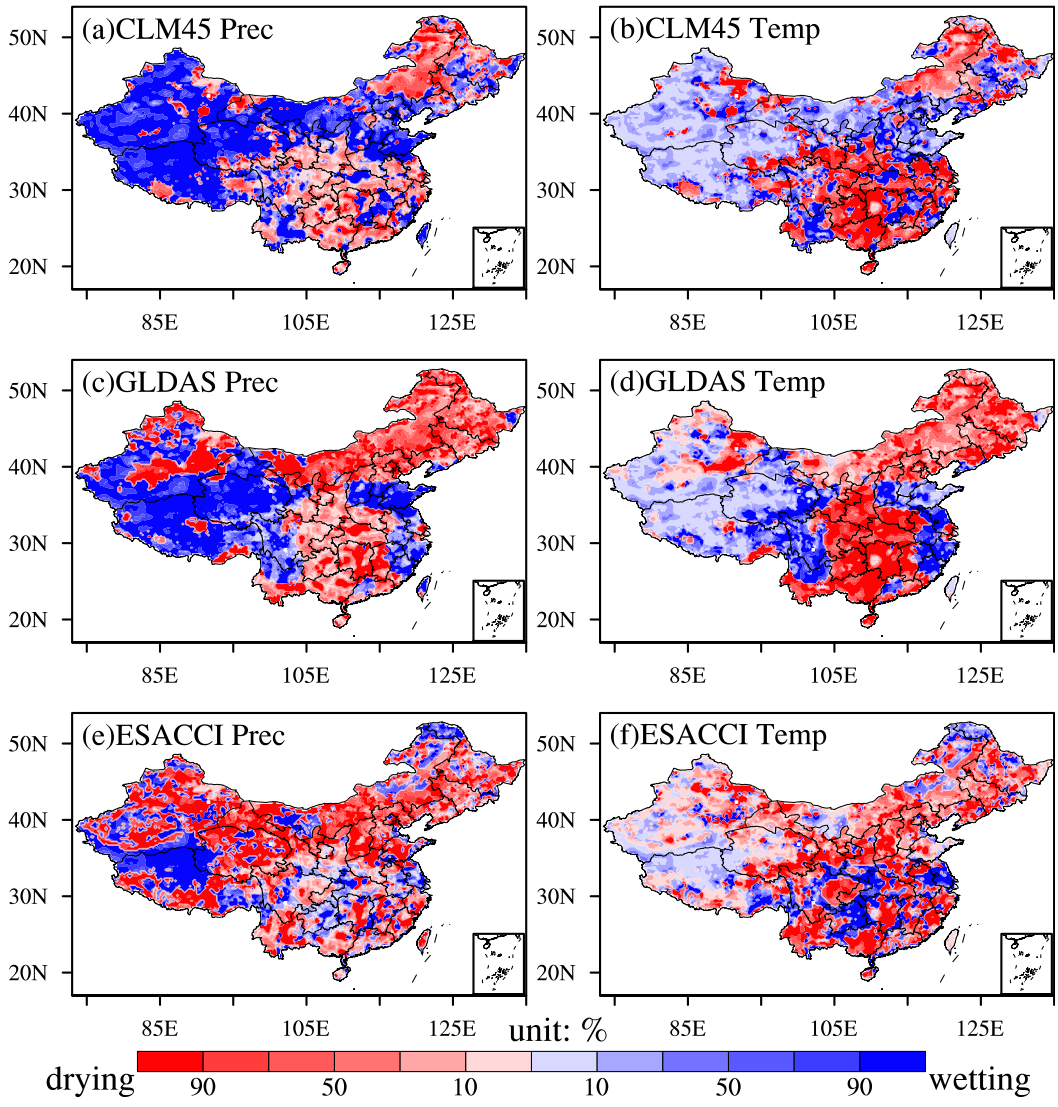


FIG. 8. The relative contribution of the changes in precipitation and temperature on soil moisture trends (%). Red (blue) colors represent drying (wetting) trends.

with ground-based measurements, the weighted average of the CLM4.5 results at 0–10 cm was computed based on the four uppermost soil layer thicknesses, while only the first layer (0–10 cm) from GLDAS was chosen in this study. Microwave observations normally measure the wetness conditions of only the top 2–5 cm (Liu et al. 2011, 2012; Dorigo et al. 2015). The mismatch in soil depths may have a negative effect on the comparison results. Moreover, the different products used to develop ESA CCI vary over space and time (Liu et al. 2012), and differences in the microwave observation channels and sampling densities are expected to influence the quality of the different periods (Albergel et al. 2013a). Various studies (Albergel et al. 2013b; Dorigo et al. 2015; Jia et al. 2015) have indicated that the ESA CCI data quality shows a stable to slightly better performance over time, except for a decline in performance during 2007–10, which may be related to the resampling and scaling strategy used to incorporate the ASCAT product (Dorigo et al. 2015). However, their potential effect on soil moisture trends is not clear. Liu et al. (2012) indicated that the ESA CCI recalling process slightly changes the absolute values of trends due to some assumptions. For example, the SMMR was assumed to have the same dynamic range with the merged SSM/I–TMI–AMSR-E, while the two active microwave products have the same cumulative distribution function curves (Liu et al. 2012). Additional work will focus on the stability of soil moisture temporal variations for the ESA CCI using

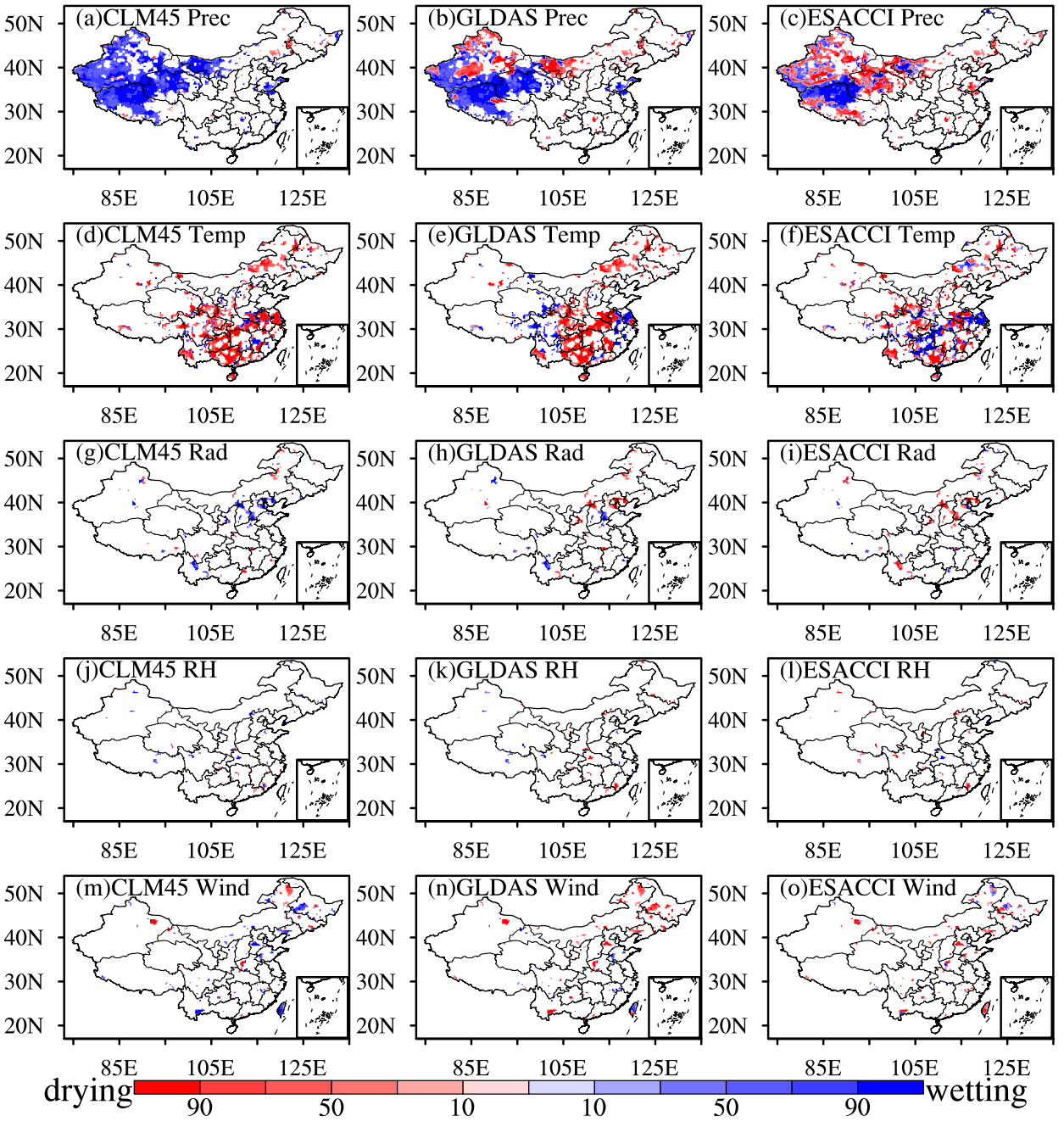


FIG. 9. As in Fig. 8, but for the relative contribution of five climate factors: (a)–(c) precipitation (Prec), (d)–(f) temperature (Temp), (g)–(i) solar radiation (Rad), (j)–(l) relative humidity (RH), and (m)–(o) wind speed (Wind) on soil moisture trends (%). Red (blue) colors represent drying (wetting) trends and only the dominant climate factor (max contribution) is shown for each grid.

the latest version V03.2, which included two new sensors and improved the merging method (http://www.esa-soilmoisture-cci.org/node/215).

Since we do not know which in situ station is located in the irrigated region and the irrigation scheme is not enabled in both of the two LSMs, the effect of anthropogenic activities on soil moisture trends derived from both in situ measurements and LSMs is not examined in this study. Qiu et al. (2016) found that the increase of the area equipped for irrigation could partly explain the significantly wetting trends for summer in the HHH Plain since precipitation did not change significantly during the study period (1996–2010). But the relative contribution of anthropogenic activities and climate change on soil moisture

trends is still not clear, which needs more attention in our future studies.

Land surface models can capture the temporal dynamics of soil moisture well when forced by high-quality atmospheric forcing data (Albergel et al. 2012), but there are still large differences in soil moisture trends between CLM4.5 and GLDAS due to different parameterizations, associated parameters, and atmospheric forcing data. Passive remote sensing products (e.g., ESA CCI) have the capability of detecting temporal trends of surface soil moisture (Chen et al. 2016), and they capture the effects of anthropogenic activities well (Qiu et al. 2016). However, they could not effectively capture temporal variations of soil moisture in densely vegetated regions. Data assimilation has been proved to be an effective tool to integrate the advantages of both remotely sensed observations and model simulations to improve soil moisture estimations (Albergel et al. 2012; de Rosnay et al. 2013; Jia et al. 2013). But its applications in detecting the interannual variations and trends of soil moisture are still scarce, limited by the length of satellite-based data. The ESA CCI product will provide us a good choice to generate globally multidecadal assimilated products of soil moisture (Albergel et al. 2017).

*Acknowledgments.* This work was funded by the National Key Research and Development Program of China (2016YFA0600203), the Key Research Program of Frontier Sciences, CAS (QYZDY-SSW-DQC012), the National Natural Science Foundation of China (Grants 41575096, 91437220, and 41405083), and the Natural Science Foundation of Hunan Province (Grant 2015JJ3098). The ESA CCI soil moisture dataset was downloaded from http://www.esa-soilmoisture-cci.org; the in situ soil moisture observations were downloaded from http://data.cma.cn/. The ITP forcing dataset used in this study was provided by the Data Assimilation and Modeling Center for Tibetan Multi-spheres, Institute of Tibetan Plateau Research, Chinese Academy of Sciences. The GLDAS data used in this study were acquired as part of the mission of NASA's Earth Science Division and archived and distributed by the Goddard Earth Sciences (GES) Data and Information Services Center (DISC). The authors thank the editor and the reviewers for their constructive comments and suggestions on the paper.

## REFERENCES

Albergel, C., P. de Rosnay, C. Gruhier, J. Muñoz-Sabater, S. Hasenauer, L. Isaksen, Y. Kerr, and W. Wagner, 2012: Evaluation of remotely sensed and modelled soil moisture products using global ground-based in situ observations. *Remote Sens. Environ.*, **118**, 215–226, https://doi.org/10.1016/j.rse.2011.11.017.

——, and Coauthors, 2013a: Monitoring multi-decadal satellite earth observation of soil moisture products through land surface reanalyses. *Remote Sens. Environ.*, **138**, 77–89, https://doi.org/10.1016/j.rse.2013.07.009.

——, W. Dorigo, R. Reichle, G. Balsamo, P. de Rosnay, J. Muñoz-Sabater, L. Isaksen, and W. Wagner, 2013b: Skill and global trend analysis of soil moisture from reanalyses and microwave remote sensing. *J. Hydrometeor.*, **14**, 1259–1277, https://doi.org/10.1175/JHM-D-12-0161.1.

——, and Coauthors, 2017: Sequential assimilation of satellite-derived vegetation and soil moisture products using SURFEX_v8.0: LDAS-Monde assessment over the Euro-Mediterranean area. *Geosci. Model Dev.*, **10**, 3889–3912, https://doi.org/10.5194/gmd-10-3889-2017.

An, R., and Coauthors, 2016: Validation of the ESA CCI soil moisture product in China. *Int. J. Appl. Earth Obs. Geoinf.*, **48**, 28–36, https://doi.org/10.1016/j.jag.2015.09.009.

Bartalis, Z., W. Wagner, V. Naeimi, S. Hasenauer, K. Scipal, H. Bonekamp, J. Figa, and C. Anderson, 2007: Initial soil moisture retrievals from the METOP-A Advanced Scatterometer (ASCAT). *Geophys. Res. Lett.*, **34**, L20401, https://doi.org/10.1029/2007GL031088.

Chen, F., and Z. Xie, 2010: Effects of interbasin water transfer on regional climate: A case study of the Middle Route of the South-to-North Water Transfer Project in China. *J. Geophys. Res.*, **115**, D11112, https://doi.org/10.1029/2009JD012611.

——, and Coauthors, 1996: Modeling of land surface evaporation by four schemes and comparison with FIFE observations. *J. Geophys. Res.*, **101**, 7251–7268, https://doi.org/10.1029/95JD02165.

Chen, X., and Coauthors, 2016: Detecting significant decreasing trends of land surface soil moisture in eastern China during the past three decades (1979–2010). *J. Geophys. Res. Atmos.*, **121**, 5177–5192, https://doi.org/10.1002/2015JD024676.

Chen, Y., K. Yang, J. He, J. Qin, J. Shi, J. Du, and Q. He, 2011: Improving land surface temperature modeling for dryland of China. *J. Geophys. Res.*, **116**, D20104, https://doi.org/10.1029/2011JD015921.

Cheng, S., X. Guan, J. Huang, F. Ji, and R. Guo, 2015: Long-term trend and variability of soil moisture over East Asia. *J. Geophys. Res. Atmos.*, **120**, 8658–8670, https://doi.org/10.1002/2015JD023206.

Dai, A., 2013: Increasing drought under global warming in observations and models. *Nat. Climate Change*, **3**, 52–58, https://doi.org/10.1038/nclimate1633.

Dai, Y., and Coauthors, 2003: The Common Land Model. *Bull. Amer. Meteor. Soc.*, **84**, 1013–1023, https://doi.org/10.1175/BAMS-84-8-1013.

de Rosnay, P., M. Drusch, D. Vasiljevic, G. Balsamo, C. Albergel, and L. Isaksen, 2013: A simplified extended Kalman filter for the global operational soil moisture analysis at ECMWF. *Quart. J. Roy. Meteor. Soc.*, **139**, 1199–1213, https://doi.org/10.1002/qj.2023.

Dorigo, W., R. De Jeu, D. Chung, R. Parinussa, Y. Liu, W. Wagner, and D. Fernandez, 2012: Evaluating global trends (1988–2010) in homogenized remotely sensed surface soil moisture. *Geophys. Res. Lett.*, **39**, L18405, https://doi.org/10.1029/2012GL052988.

——, and Coauthors, 2015: Evaluation of the ESA CCI soil moisture product using ground-based observations. *Remote Sens. Environ.*, **162**, 380–395, https://doi.org/10.1016/j.rse.2014.07.023.

——, and Coauthors, 2017: ESA CCI soil moisture for improved Earth system understanding: State-of-the art and future directions. *Remote Sens. Environ.*, **203**, 185–215, https://doi.org/10.1016/j.rse.2017.07.001.

Feng, H., and M. Zhang, 2015: Global land moisture trends: Drier in dry and wetter in wet over land. *Sci. Rep.*, **5**, 18018, https://doi.org/10.1038/srep18018.

Guo, Z., P. A. Dirmeyer, Z. Z. Hu, X. Gao, and M. Zhao, 2006: Evaluation of the Second Global Soil Wetness Project soil moisture simulations: 2. Sensitivity to external meteorological forcing. *J. Geophys. Res.*, **111**, D22S03, https://doi.org/10.1029/2006JD007845.

Huang, J., T. Wang, W. Wang, Z. Li, and H. Yan, 2014: Climate effects of dust aerosols over East Asian arid and semiarid regions. *J. Geophys. Res. Atmos.*, **119**, 11 398–11 416, https://doi.org/10.1002/2014JD021796.

Huang, M., Z. Hou, L. Leung, Y. Ke, Y. Liu, Z. Fang, and Y. Sun, 2013: Uncertainty analysis of runoff simulations and parameter identifiability in the Community Land Model: Evidence from MOPEX basins. *J. Hydrometeor.*, **14**, 1754–1772, https://doi.org/10.1175/JHM-D-12-0138.1.

Jia, B., X. Tian, Z. Xie, J. Liu, and C. Shi, 2013: Assimilation of microwave brightness temperature in a land data assimilation system with multi-observation operators. *J. Geophys. Res. Atmos.*, **118**, 3972–3985, https://doi.org/10.1002/jgrd.50377.

——, J. Liu, and Z. Xie, 2015: Evaluation of a multi-satellite soil moisture product and the Community Land Model 4.5 simulation in China. *Hydrol. Earth Syst. Sci. Discuss.*, **12**, 5151–5186, https://doi.org/10.5194/hessd-12-5151-2015.

Lai, X., J. Wen, S. Cen, X. Huang, H. Tian, and X. Shi, 2016: Spatial and temporal soil moisture variations over China from simulations and observations. *Adv. Meteor.*, **2016**, 4587687, https://doi.org/10.1155/2016/4587687.

Li, M., Z. Ma, and G. Niu, 2011: Modeling spatial and temporal variations in soil moisture in China. *Chin. Sci. Bull.*, **56**, 1809–1820, https://doi.org/10.1007/s11434-011-4493-0.

Li, X., X. Gao, J. Wang, and H. Guo, 2015: Microwave soil moisture dynamics and response to climate change in central Asia and Xinjiang Province, China, over the last 30 years. *J. Appl. Remote Sens.*, **9**, 096012, https://doi.org/10.1117/1.JRS.9.096012.

Liu, J., and Z. Xie, 2013: Improving simulation of soil moisture in China using a multiple meteorological forcing ensemble approach. *Hydrol. Earth Syst. Sci.*, **17**, 3355–3369, https://doi.org/10.5194/hess-17-3355-2013.

——, B. Jia, Z. Xie, and C. Shi, 2016: Ensemble simulation of land evapotranspiration in China based on a multi-forcing and multi-model approach. *Adv. Atmos. Sci.*, **33**, 673–684, https://doi.org/10.1007/s00376-016-5213-0.

Liu, Y., R. Parinussa, W. Dorigo, R. De Jeu, W. Wagner, A. van Dijk, M. McCabe, and J. Evans, 2011: Developing an improved soil moisture dataset by blending passive and active microwave satellite-based retrievals. *Hydrol. Earth Syst. Sci.*, **15**, 425–436, https://doi.org/10.5194/hess-15-425-2011.

——, W. Dorigo, R. Parinussa, R. De Jeu, W. Wagner, M. McCabe, J. Evans, and A. van Dijk, 2012: Trend-preserving blending of passive and active microwave soil moisture retrievals. *Remote Sens. Environ.*, **123**, 280–297, https://doi.org/10.1016/j.rse.2012.03.014.

——, W. Guo, and Y. Song, 2016: Estimation of key surface parameters in semi-arid region and their impacts on improvement of surface fluxes simulation. *Sci. China Earth Sci.*, **59**, 307–319, https://doi.org/10.1007/s11430-015-5140-4.

Loew, A., T. Stacke, W. Dorigo, R. de Jeu, and S. Hagemann, 2013: Potential and limitations of multidecadal satellite soil moisture observations for selected climate model evaluation studies. *Hydrol. Earth Syst. Sci.*, **17**, 3523–3542, https://doi.org/10.5194/hess-17-3523-2013.

Njoku, E., T. Jackson, V. Lakshmi, T. Chan, and S. Nghiem, 2003: Soil moisture retrieval from AMSR-E. *IEEE Trans. Geosci. Remote Sens.*, **41**, 215–229, https://doi.org/10.1109/TGRS.2002.808243.

Oleson, K., and Coauthors, 2013: Technical description of version 4.5 of the Community Land Model (CLM). NCAR Tech. Note NCAR/TN-503+STR, 420 pp., https://doi.org/10.5065/D6RR1W7M.

Qiu, J., Q. Gao, S. Wang, and Z. Su, 2016: Comparison of temporal trends from multiple soil moisture data set sand precipitation: The implication of irrigation on regional soil moisture trend. *Int. J. Appl. Earth Obs. Geoinf.*, **48**, 17–27, https://doi.org/10.1016/j.jag.2015.11.012.

Rahmani, A., S. Golian, and L. Brocca, 2016: Multiyear monitoring of soil moisture over Iran through satellite and reanalysis soil moisture products. *Int. J. Appl. Earth Obs. Geoinf.*, **48**, 85–95, https://doi.org/10.1016/j.jag.2015.06.009.

Robock, A., and H. Li, 2006: Solar dimming and $CO_2$ effects on soil moisture trends. *Geophys. Res. Lett.*, **33**, L20708, https://doi.org/10.1029/2006GL027585.

Rodell, M., and Coauthors, 2004: The Global Land Data Assimilation System. *Bull. Amer. Meteor. Soc.*, **85**, 381–394, https://doi.org/10.1175/BAMS-85-3-381.

Sen, P. K., 1968: Estimates of the regression coefficient based on Kendall's tau. *J. Amer. Stat. Assoc.*, **63**, 1379–1389.

Seneviratne, S., T. Corti, E. Davin, M. Hirschi, E. Jaeger, I. Lehner, B. Orlowsky, and A. Teuling, 2010: Investigating soil moisture–climate interactions in a changing climate: A review. *Earth-Sci. Rev.*, **99**, 125–161, https://doi.org/10.1016/j.earscirev.2010.02.004.

Sheffield, J., and E. Wood, 2008: Global trends and variability in soil moisture and drought characteristics, 1950–2000, from observation-driven simulations of the terrestrial hydrologic cycle. *J. Climate*, **21**, 432–458, https://doi.org/10.1175/2007JCLI1822.1.

——, G. Goteti, and E. Wood, 2006: Development of a 50-year high-resolution global dataset of meteorological forcings for land surface modeling. *J. Climate*, **19**, 3088–3111, https://doi.org/10.1175/JCLI3790.1.

Shi, W., F. Tao, and J. Liu, 2014: Regional temperature change over the Huang-Huai-Hai Plain: The roles of irrigation versus urbanization. *Int. J. Climatol.*, **34**, 1181–1195, https://doi.org/10.1002/joc.3755.

Su, C. H., D. Ryu, W. A. Dorigo, S. Zwieback, A. Gruber, C. Albergel, R. H. Reichle, and W. Wagner, 2016: Homogeneity of a global multi-satellite soil moisture climate data record. *Geophys. Res. Lett.*, **43**, 11 245–11 252, https://doi.org/10.1002/2016GL070458.

Wang, A., and X. Zeng, 2011: Sensitivities of terrestrial water cycle simulations to the variations of precipitation and air temperature in China. *J. Geophys. Res.*, **116**, D02107, https://doi.org/10.1029/2010JD014659.

——, D. Lettenmaier, and J. Sheffield, 2011: Soil moisture drought in China, 1950–2006. *J. Climate*, **24**, 3257–3271, https://doi.org/10.1175/2011JCLI3733.1.

Wang, S., X. Mo, S. Liu, Z. Lin, and S. Hu, 2016: Validation and trend analysis of ECV soil moisture data on cropland in North China Plain during 1981–2010. *Int. J. Appl. Earth Obs. Geoinf.*, **48**, 110–121, https://doi.org/10.1016/j.jag.2015.10.010.

Yang, K., J. He, W. Tang, J. Qin, and C. Cheng, 2010: On downward shortwave and longwave radiations over high altitude regions: Observation and modeling in the Tibetan

Plateau. *Agric. For. Meteor.*, **150**, 38–46, https://doi.org/10.1016/j.agrformet.2009.08.004.

Yuan, X., Z. Ma, M. Pan, and C. Shi, 2015: Microwave remote sensing of short-term droughts during crop growing seasons. *Geophys. Res. Lett.*, **42**, 4394–4401, https://doi.org/10.1002/2015GL064125.

Zeng, Y., Z. Xie, Y. Yu, S. Liu, L. Wang, J. Zou, P. Qin, and B. Jia, 2016: Effects of anthropogenic water regulation and groundwater lateral flow on land processes. *J. Adv. Model. Earth Syst.*, **8**, 1106–1131, https://doi.org/10.1002/2016MS000646.

Zhan, X., W. Zheng, L. Fang, J. Liu, C. Hain, J. Yin, and M. Ek, 2016: A preliminary assessment of the impact of SMAP soil moisture on numerical weather forecasts from GFS and NUWRF models. *2016 IEEE Int. Geoscience and Remote Sensing Symp.*, Beijing, China, IEEE, 5229–5232, https://doi.org/10.1109/IGARSS.2016.7730362.

Zhao, Y., J. Zhu, and Y. Xu, 2014: Establishment and assessment of the grid precipitation datasets in China for recent 50 years (in Chinese). *J. Meteor. Sci.*, **34**, 414–420.

Zheng, X., K. Zhao, Y. Ding, T. Jiang, S. Zhang, and M. Jin, 2016: The spatiotemporal patterns of surface soil moisture in Northeast China based on remote sensing products. *J. Water Climate Change*, **7**, 708–720, https://doi.org/10.2166/wcc.2016.106.